Journal of Solid State Chemistry 181 (2008) 2433–2441

Contents lists available at ScienceDirect

Journal of Solid State Chemistry

journal homepage: www.elsevier.com/locate/jssc

New germanates RCrGeO$_5$ (R = Nd–Er, Y): Synthesis, structure, and properties

Roman V. Shpanchenko [a,d,*], Alexander A. Tsirlin [a], Ekaterina S. Kondakova [a], Evgeny V. Antipov [a], Catherine Bougerol [b], Joke Hadermann [c], Gustaaf van Tendeloo [c], Hiroya Sakurai [d], Eiji Takayama-Muromachi [d]

[a] Department of Chemistry, Moscow State University, Leninskie Gory, Moscow 119992, Russia
[b] Nanophysique et Semiconducteurs Group, CNRS-Institut Néel and CEA-INAC-SP2M, 17 rue des martyrs, 38054 Grenoble Cedex 9, France
[c] EMAT, University of Antwerp, Groenenborgerlaan 171, Antwerp B-2020, Belgium
[d] NIMS, 1-1 Namiki, Tsukuba, Ibaraki 305-0044, Japan

ARTICLE INFO

Article history:
Received 26 January 2008
Received in revised form
23 May 2008
Accepted 27 May 2008
Available online 5 June 2008

Keywords:
Chromium germanium oxide
Crystal structure
Magnetic properties

ABSTRACT

The new complex germanates RCrGeO$_5$ (R = Nd–Er, Y) have been synthesized and investigated by means of X-ray powder diffraction, electron microscopy, magnetic susceptibility and specific heat measurements. All the compounds are isostructural and crystallize in the orthorhombic symmetry, space group *Pbam*, and $Z = 4$. The crystal structure of RCrGeO$_5$, as refined using X-ray powder diffraction data, includes infinite chains built by edge-sharing $Cr^{+3}O_6$ octahedra with two alternating Cr–Cr distances. The chains are combined into a three-dimensional framework by Ge_2O_8 groups consisting of two edge-linked square pyramids oriented in opposite directions. The resulting framework contains pentagonal channels where rare-earth elements are located. Thus, RCrGeO$_5$ germanates present new examples of RMn$_2$O$_5$-type compounds and show ordering of Cr^{+3} and Ge^{+4} cations. Electron diffraction as well as high-resolution electron microscopy confirm the structure solution. Magnetic susceptibility data for R = Nd, Sm, and Eu are qualitatively consistent with the presence of isolated 3*d* (antiferromagnetically coupled Cr^{+3} cations) and 4*f* (R^{+3}) spin subsystems in the RCrGeO$_5$ compounds. NdCrGeO$_5$ undergoes long-range magnetic ordering at 2.6 K, while SmCrGeO$_5$ and EuCrGeO$_5$ do not show any phase transitions down to 2 K.

1. Introduction

Complex manganese oxides RMn$_2$O$_5$ (R = Y, Bi, or rare-earth cations) have recently attracted considerable attention due to an unusual magnetoelectric effect [1–9]. The key feature of these compounds deals with magnetic frustration resulting in a number of phase transitions to ordered (commensurately or incommensurately) spin states, while some of these states give rise to polar structural distortions and ferroelectricity. Thus, the physics of RMn$_2$O$_5$ is controlled by the magnitudes of competing magnetic interactions, whereas the interactions depend on structural parameters and, in particular, on the size of the R cation. Large R cations (La, Bi) provide relatively simple commensurate magnetic structures [10,11]. Smaller cations (Y, Sm–Lu) give rise to more complicated spin states and magnetic field-controlled ferroelectricity [12].

The temperature of the ferroelectric transitions in the RMn$_2$O$_5$ compounds is rather low (30–40 K), and the realization of the magnetoelectric effect in these systems at higher temperatures remains a challenging problem. One may think that the substitution of manganese by other transition metal cations will modify the spin system hence leading to higher transition temperatures. Indeed, the temperatures of long-range magnetic ordering of RFeMnO$_5$ (R = Y, Ho, Er) are enhanced as compared with that of RMn$_2$O$_5$. However, the RFeMnO$_5$ compounds are weakly frustrated, since different relevant orbitals of the penta-coordinated cation (Fe^{+3} in RFeMnO$_5$ and Mn^{+3} in RMn$_2$O$_5$) give rise to magnetic interactions of different sign. Moreover, a partial Fe/Mn disorder is present, and the RFeMnO$_5$ oxides do not show ferroelectricity [13]. Another RMn$_2$O$_5$-type compound, YCrMnO$_5$, strongly suffers from Cr/Mn disorder and is also unsuitable for the purpose formulated above [14]. Nevertheless, the search for new RMn$_2$O$_5$-type compounds is of high importance, if one succeeds to combine two cations giving rise to magnetic frustration, and to provide complete ordering of these cations within the RMn$_2$O$_5$ structure.

To realize the RMn$_2$O$_5$-type structure, it is necessary to choose two different cations M' and M'' having stable octahedral and

* Corresponding author at: Department of Chemistry, Moscow State University, Leninskie Gory, Moscow 119992, Russia. Fax: +7 095 939 47 88.
E-mail address: shpanchenko@icr.chem.msu.ru (R.V. Shpanchenko).

0022-4596/$ - see front matter © 2008 Elsevier Inc. All rights reserved.
doi:10.1016/j.jssc.2008.05.043

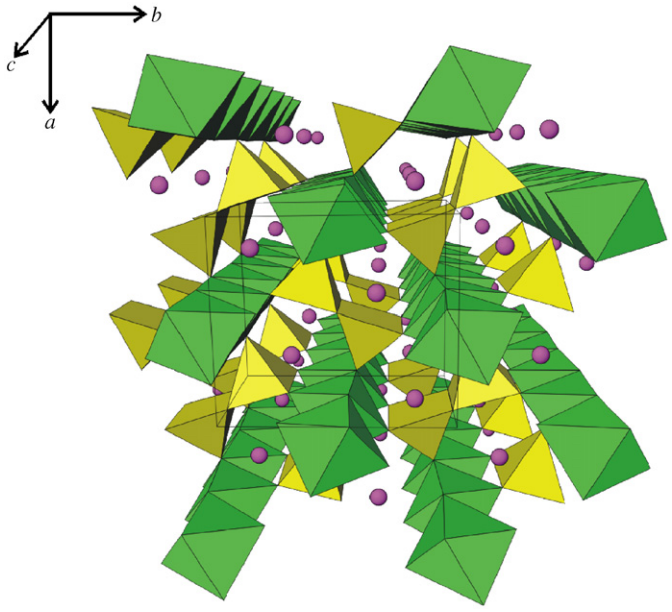

Fig. 1. The overall view of the RCrGeO$_5$ crystal structure. Chromium (M'-type) atoms are situated in the octahedra and germanium ones (M''-type) are situated in the square pyramids connected via the common edge. The circles represent rare-earth atoms.

square pyramidal coordination, respectively (see Fig. 1). Basically, the choice of the cations is not limited by transition metals only. For example, RAlGeO$_5$ compounds include Al as M' and Ge as M'' [15,16], while YGa$_{1-x}$Mn$_{1+x}$O$_5$ contains Ga atoms that predominantly occupy the square-pyramidal position [17]. In our study, we try another combination of the cations and use Cr^{+3} as M' due to its high stability in air. As for M'', we choose Ge^{+4}. The substitution of Mn atoms in RMn$_2$O$_5$ by magnetic Cr^{+3} and non-magnetic Ge^{+4} results in a series of novel compounds RCrGeO$_5$. We study the prepared compounds with X-ray powder diffraction (XPD), electron microscopy, magnetic susceptibility and specific heat measurements focusing on the details of the crystal structure. Next, we use the structural data to discuss the factors influencing the stability of the RMn$_2$O$_5$ structure and suggest new ideas for combining appropriate transition metal cations within this structure type.

2. Experimental

Bulk powder samples of RCrGeO$_5$ (R = Nd–Er, Y) were obtained by solid-state reaction of stoichiometric mixtures of R_2O_3, Cr_2O_3, and GeO_2 in air for 2 weeks at 1250 °C with several intermediate grindings. Initial oxides were intimately grinded in an agate mortar under acetone, pressed into pellets and placed into alumina crucibles. After 1 week of annealing only RCrGeO$_5$ and RCrO$_3$ (about 5 wt%) were found in the reaction mixture. The formation of the RCrO$_3$ impurity implies the lack of GeO_2, likely due to its volatilization at high temperature. Therefore, at this stage an appropriate amount of GeO_2 calculated from the RCrGeO$_5$ stoichiometry was added to the samples, and a further annealing for 1 week was performed. Finally, we succeeded to prepare single-phase samples for R = Nd, Sm, and Eu, while the samples with R = Gd–Er, Y always contained admixtures (usually RCrO$_3$ and $R_2Ge_2O_7$; the total amount of the impurities did not exceed 7 wt%). An increase of the annealing temperature up to 1300 °C or longer annealings at 1250 °C resulted in partial decomposition of all the compounds with the formation of ternary oxides. No traces of melt were detected. Synthesis with R = La–Pr and Tm–Lu always resulted in multiphase mixtures, and no RCrGeO$_5$-type phase could be found.

XPD data for the structure refinement were collected on the STADI P (Cu$K\alpha_1$-radiation, linear PSD) and RINT2000 (Cu$K\alpha$-radiation, scintillation counter) diffractometers. GSAS program package [18] was used for the Rietveld structure refinement.

Transmission electron microscopy was performed with a Philips CM20 microscope [electron diffraction (ED)] equipped with a LINK 2000 attachment and with a JEOL 4000EX microscope [ED and high-resolution electron microscopy (HREM)]. The image simulations were made using JEMS software.

Magnetic susceptibility was measured by a commercial SQUID magnetometer (MPMS-XL, Quantum Design). The measurements were done under field-cooling condition in fields $\mu_0 H$ of 0.1 and 1 T in a temperature range of 1.8–400 K. Specific heat measurement was done using the PPMS (Quantum Design) device at zero field.

3. Results

3.1. Crystal structure of the $RCrGeO_5$ compounds

X-ray patterns for all the RCrGeO$_5$ compounds are very similar. The patterns were indexed in orthorhombic symmetry with lattice parameters listed in Table 1. The analysis of the systematic extinctions allowed us to suggest the *Pbam* space group similar to the RMn$_2$O$_5$ phases (R = La–Lu, Y) [20]. This conclusion was confirmed by ED study (see below). We failed to obtain single crystals of RCrGeO$_5$ due to phase decomposition above 1300 °C. Therefore, the crystal structures were refined using XPD data. The starting atomic coordinates were taken from the NdMn$_2$O$_5$ structure [21]. The refinement revealed that chromium atoms were situated in the octahedral positions, whereas germanium atoms occupied the square pyramids, i.e., cation ordering was realized. Such a separation of the chromium and germanium atoms in different crystallographic positions resulted in the best fit, and the refinement of their occupancies yielded 1.0 within the standard deviations. The cation ordering in RCrGeO$_5$ looks reasonable, since the square-pyramidal coordination is rather typical for Ge^{4+} (see below) and atypical for Cr^{+3} (only two structures are known: Sr_2CuCrO_3S [22] and $Cr(H_2O)_5(NO)(SO_4)$ [23]). Displacement parameters for oxygen atoms were constrained, and those for the other atoms were refined independently.

The crystallographic and experimental parameters as well as the resulting atomic coordinates are listed in Tables 2 and 3, respectively, for EuCrGeO$_5$ as a representative example of the RCrGeO$_5$ compounds. Experimental, calculated, and difference X-ray patterns for EuCrGeO$_5$ are shown in Fig. 2. The structural data for the other compounds can be found in the Supplementary

Table 1
Lattice parameters, cell volume, and ionic radii of the rare-earth cations [19] for RCrGeO$_5$

R	a (Å)	b (Å)	c (Å)	V (Å^3)	r_R (Å)
Nd	7.51926 (8)	8.53474 (9)	5.74493 (6)	368.68	1.26
Sm	7.46501 (7)	8.49553 (7)	5.72217 (5)	362.90	1.23
Eu	7.4389 (1)	8.4798 (2)	5.7169 (1)	360.62	1.21
Gd	7.4130 (3)	8.4661 (3)	5.7100 (2)	358.36	1.20
Tb	7.3899 (3)	8.4457 (4)	5.6986 (3)	355.67	1.18
Dy	7.3661 (2)	8.4269 (2)	5.6936 (1)	353.42	1.17
Ho	7.3444 (1)	8.4128 (1)	5.6874 (1)	351.41	1.16
Er	7.3245 (1)	8.3979 (2)	5.6815 (1)	349.47	1.14
Y	7.34210 (7)	8.41283 (7)	5.68314 (5)	351.04	1.155

Information. The interatomic distances and angles relevant for the further discussion are listed in Table 4 for all the compounds under investigation.

The crystal structure of RCrGeO$_5$ is shown in Fig. 1. It contains infinite chains of edge-sharing CrO$_6$ octahedra running along the c-axis. The chains are interconnected by Ge$_2$O$_8$ units (two edge-sharing square pyramids) to form a three-dimensional framework with pentagonal tunnels parallel to the chains of the octahedra. The rare-earth cations are located inside these tunnels. Bond valence sum calculations [24] confirmed the oxidation states as 3, 3, and 4 for R, Cr, and Ge atoms, respectively, in all the refined structures. No sign of Cr/Ge disorder is observed from the XPD data.

Chromium atoms are situated in almost regular octahedra. Two apical Cr–O(4) bonds (1.99–2.02 Å) are slightly elongated as compared with four equatorial ones (1.93–2.00 Å). The Cr–O(4) distance is almost independent on the R cation (see Table 4), while the four other distances are more changeable due to the variation of Cr–Cr separations (see below).

Germanium atoms have a square pyramidal coordination. The apical Ge–O(3) distance (1.71–1.80 Å) is slightly shorter than the four equatorial ones (1.81–1.87 and 1.87–1.93 Å) due to the shift of the germanium atom from the base of the pyramid. One should note that Ge–O separations found in this study are close to those in the other structures and somewhat shorter than Cr–O distances in the Cr^{+3}O$_5$ square pyramids [22,23]. This result further points out the cation ordering in RCrGeO$_5$. There is no clear trend in the change of the Ge–O distances with the variation of the R cation. The pyramids are rather flexible and fit the structural alterations caused by the R cations and the Cr chains. Two pyramids oriented in opposite directions share their O(1)–O(1) edge and give rise to the Ge$_2$O$_8$ structural units. The formation of such dimers is not common for germanium oxides, although several examples have been reported: besides RAlGeO$_5$ [15,16], they are La$_3$GaGe$_5$O$_{16}$ [25], CaCuGe$_2$O$_6$ [26], and K$_2$Ge$_8$O$_{17}$ [27].

Rare-earth cations have 8-fold coordination as shown in Fig. 3. The resulting RO$_8$ polyhedra share edges and corners forming layers in the ab plane. The averaged R–O distances are decreased from Nd to Y consistent with the reduction of the ionic radius.

The CrO$_6$ octahedra share their opposite O(2)–O(2) and O(3)–O(3) edges to form rutile-like chains as shown in Fig. 4. The Cr–Cr separations within the chain are not equal. So, the Cr–Cr separation via the O(2)–O(2) edge (D_1) is noticeably longer than that via the O(3)–O(3) edge (D_2). Moreover, D_2 is nearly constant, while D_1 is reduced as the R cation gets smaller (see Table 4 and Section 4). This difference results from the constraint imposed by the O(4)–O(4) edge of the GeO$_5$ square pyramid. Note that D_2 is close to the Cr–Cr distance that is typically observed in the chains of edge-sharing CrO$_6$ octahedra (see, for example, [28]), while D_1 is considerably shorter.

The intra-chain Cr–Cr separations bear influence on the equatorial Cr–O distances and the respective interatomic angles. The longer separation D_1 corresponds to the larger Cr–O(2)–Cr angle (93–98°), and the shorter separation D_2 reveals the smaller Cr–O(3)–Cr angle (88–93°). Similar to D_1 and D_2, the Cr–O(2) distances (1.93–2.00 Å) are more changeable as compared with the Cr–O(3) ones (1.93–1.97 Å). Yet in contrast to D_1 and D_2, neither the angles nor the Cr–O distances show a clear trend with the change of the R cation. One may think that these individual geometrical parameters are rather flexible within the general constraints imposed by the Cr–Cr separations.

Table 2
Experimental and crystallographic parameters for EuCrGeO$_5$

Composition	EuCrGeO$_5$
Formula weight	356.54
Space group (no.)	*Pbam* [55]
A (Å)	7.4389 (1)
B (Å)	8.4798 (2)
C (Å)	5.7169 (1)
Z	4
V (Å^3)	360.62 (2)
Calculated density (g/cm^3)	6.567
μ (mm^{-1})	38.77
Color	Pale-green
Diffractometer	RINT2000, Rigaku
Radiation, wavelength (Å)	Cu$K\alpha$, 1.54
Detector	Scintillation
Refinement method	Full-profile (Rietveld)
Program used	GSAS
Number of atomic sites	8
No. of variables	45
2θ range, step (deg)	10–110, 0.02
Total number of profile points	5000
R_{wp}, R_p, χ^2	0.077, 0.054, 2.26

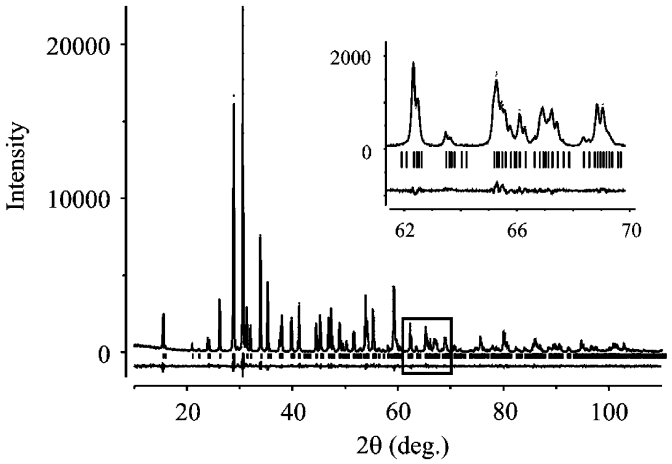

Fig. 2. Experimental, calculated, and difference X-ray patterns for EuCrGeO$_5$.

Table 3
Atomic coordinates and displacement parameters for EuCrGeO$_5$

Atom	Position	x	y	z	$U_{iso} \times 100$ (Å^2)	BVS
Eu	4g	0.14477 (9)	0.17387 (10)	0	1.08 (8)	2.9
Cr	4f	0	1/2	0.2568 (4)	0.57 (9)	3.2
Ge	4h	0.38648 (15)	0.35708 (15)	1\2	0.63 (10)	4.0
O(1)	4e	0	0	0.2993 (12)	0.30 (13)	
O(2)	4g	0.1634 (9)	0.4463 (7)	0	0.30	
O(3)	4h	0.1578 (9)	0.4252 (7)	1\2	0.30	
O(4)	8i	0.3999 (5)	0.2180 (5)	0.2601 (7)	0.30	

Table 4
Main interatomic distances (Å) and angles (deg) for the RCrGeO$_5$ compounds

R	Nd	Sm	Eu	Gd	Tb	Dy	Ho	Er	Y
R–2 × O(1)	2.513 (6)	2.502 (5)	2.502 (5)	2.458 (15)	2.457 (12)	2.441 (12)	2.435 (11)	2.392 (13)	2.406 (4)
R–O(2)	2.341 (8)	2.328 (6)	2.314 (6)	2.339 (17)	2.300 (14)	2.286 (13)	2.317 (12)	2.278 (14)	2.267 (5)
R–O(2)	2.420 (9)	2.395 (7)	2.400 (6)	2.387 (18)	2.363 (15)	2.374 (14)	2.360 (13)	2.348 (15)	2.403 (5)
R–2 × O(4)	2.464 (6)	2.430 (4)	2.440 (4)	2.366 (12)	2.370 (10)	2.371 (9)	2.380 (8)	2.355 (10)	2.366 (3)
R–2 × O(4)	2.542 (5)	2.523 (4)	2.524 (4)	2.503 (11)	2.511 (9)	2.519 (9)	2.488 (8)	2.516 (10)	2.508 (3)
Cr–2 × O(2)	1.959 (6)	1.967 (5)	1.960 (4)	1.952 (14)	2.001 (11)	1.966 (11)	1.930 (10)	1.980 (12)	1.934 (4)
Cr–2 × O(3)	1.959 (6)	1.938 (5)	1.927 (5)	1.974 (14)	1.965 (11)	1.945 (11)	1.934 (11)	1.942 (13)	1.941 (4)
Cr–2 × O(4)	2.018 (6)	2.006 (4)	1.993 (4)	1.999 (12)	1.992 (10)	1.994 (10)	1.995 (9)	1.990 (11)	1.988 (4)
Cr–O(2)–Cr	98.3 (4)	97.3 (3)	97.0 (3)	98.6 (9)	94.7 (7)	94.8 (7)	96.3 (6)	93.0 (7)	95.9 (3)
Cr–O(3)–Cr	90.4 (4)	91.3 (3)	92.3 (3)	88.3 (9)	89.0 (7)	92.0 (7)	93.3 (7)	92.6 (8)	92.8 (3)
Cr–Cr (D_1)	2.964 (6)	2.952 (4)	2.937 (4)	2.961 (15)	2.942 (12)	2.894 (11)	2.875 (12)	2.873 (14)	2.872 (4)
Cr–Cr (D_2)	2.781 (6)	2.770 (4)	2.780 (4)	2.749 (15)	2.756 (12)	2.799 (11)	2.813 (12)	2.809 (14)	2.811 (4)
Ge–2 × O(1)	1.890 (6)	1.884 (4)	1.870 (4)	1.898 (14)	1.904 (11)	1.902 (11)	1.906 (9)	1.929 (13)	1.926 (4)
Ge–O(3)	1.777 (9)	1.780 (7)	1.796 (7)	1.707 (20)	1.709 (16)	1.747 (16)	1.764 (15)	1.739 (18)	1.755 (6)
Ge–2 × O(4)	1.813 (6)	1.821 (4)	1.812 (4)	1.869 (12)	1.834 (10)	1.823 (10)	1.814 (9)	1.823 (10)	1.823 (3)
Ge–Ge	2.970 (3)	2.965 (3)	2.954 (3)	2.953 (8)	2.979 (7)	2.942 (7)	2.965 (6)	2.931 (7)	2.936 (2)

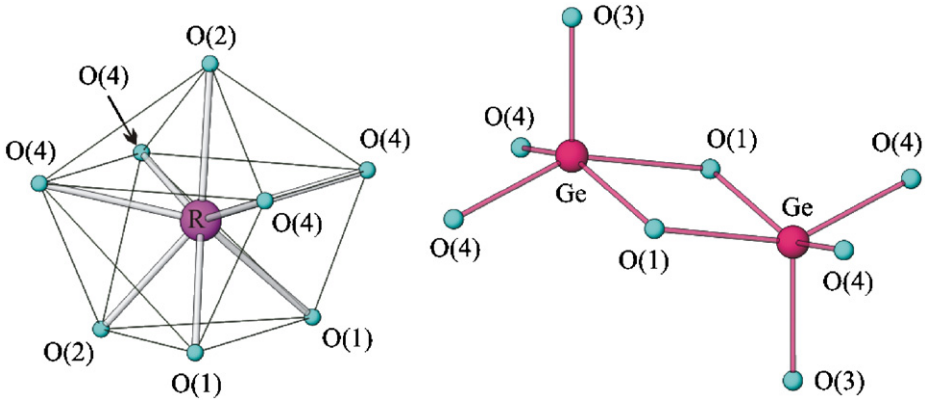

Fig. 3. Ge_2O_8 group (right panel) and coordination polyhedron for the R cation (left panel) in the RCrGeO$_5$ structure.

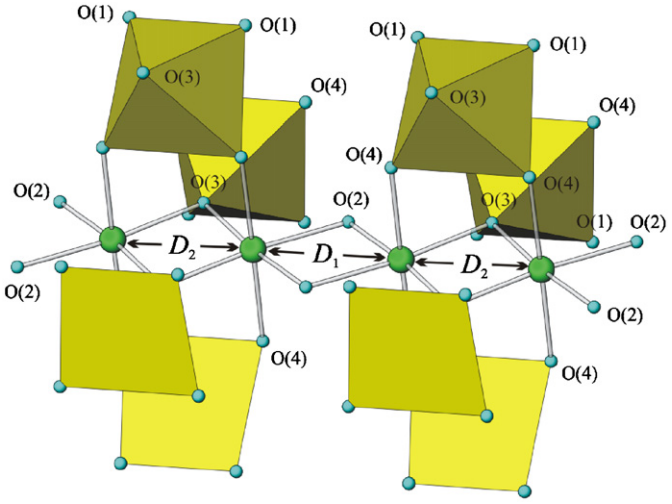

Fig. 4. A part of the RCrGeO$_5$ structure showing Cr–Cr separations in the chain of edge-sharing CrO$_6$ octahedra and the constraining effect of GeO$_5$ square pyramids.

3.2. ED and HREM study

To confirm the cell parameters and the space group deduced from the XPD data, we performed electron microscopy study. This study was carried out for NdCrGeO$_5$ only. ED patterns were obtained along the major zone axes. All the patterns are consistent with the *Pbam* space group and the lattice parameters obtained from XPD. By tilting around the main axes, the whole reciprocal space was investigated. No superstructure reflections were observed, and the patterns also did not show diffuse streaking that could be related to the presence of eventual planar defects in the structure.

Fig. 5 shows the ED patterns for [100], [010], and [001] zone axes. Forbidden reflections $h\,0\,0$ and $0\,k\,0$ with h and k odd are due to double diffraction since they disappear by tilting out of the zone axis condition.

High-resolution images were taken along the main zone axes. The images were simulated using the structural model proposed from X-ray analysis and different values of defocus and sample thickness.

The upper panel of Fig. 6 shows a HREM image along [001] with the simulated image in the inset (sample thickness of 23 nm and a defocus of 15 nm). The bottom panel of Fig. 6 presents an enlargement of the simulated and experimental images with the projected structure superimposed. Under the given conditions, the cations are clearly imaged as bright dots. Perfect correspondence of the experimental and simulated images confirms the proposed structural model.

3.3. Magnetic properties

Below, we present magnetic susceptibility data for three of the prepared germanates (with R = Nd, Sm, and Eu). Unfortunately,

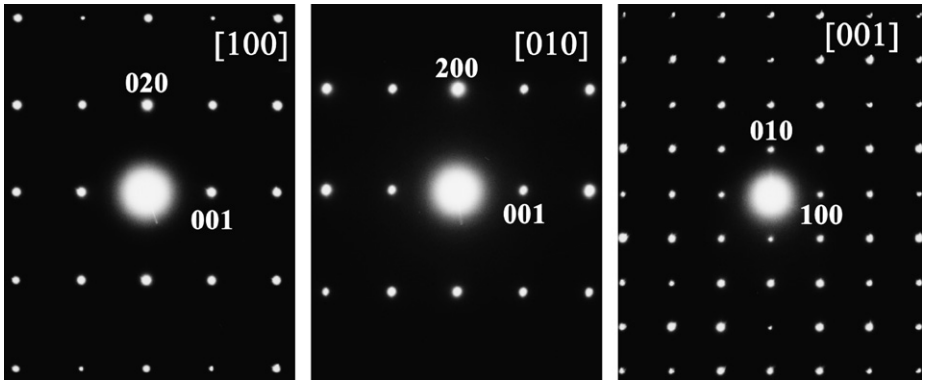

Fig. 5. Electron diffraction patterns along three main directions of $NdCrGeO_5$.

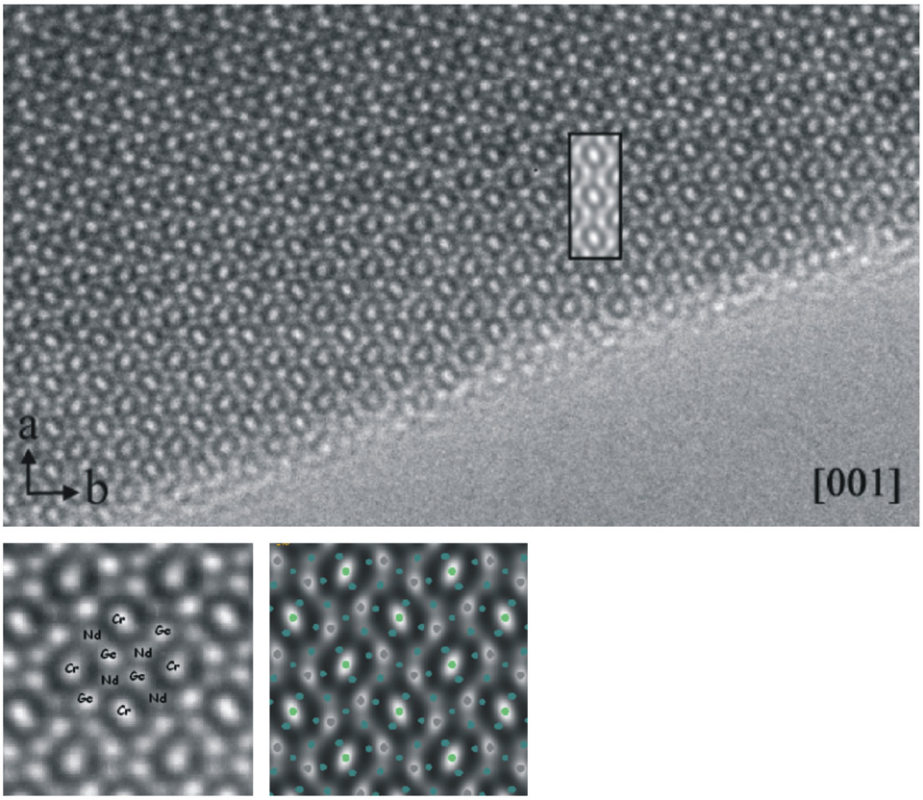

Fig. 6. Upper panel: high-resolution electron microscopy image of $NdCrGeO_5$, the rectangle shows the image simulation (details are given in the text). Bottom panel: an enlargement of the experimental (left) and simulated (right) images with the projected structure superimposed.

the data for the other compounds (R = Gd–Er, Y) were dominated by the signal of $RCrO_3$ impurities that reveal weak ferromagnetic moment below 150–200 K [29], and the contribution of $RCrGeO_5$ could not be singled out.

Magnetic susceptibility curves for $RCrGeO_5$ with R = Sm, Eu, and Nd are shown in Figs. 7–9, respectively. Three compounds reveal considerably different magnetic behavior. The curves for R = Sm and Eu are smooth indicating the lack of long-range spin ordering, while a sharp bend of the susceptibility of $NdCrGeO_5$ at $T_N = 2.6$ K corresponds to the magnetic phase transition. The long-range ordering in the neodymium compound is likely antiferromagnetic as evidenced by the decrease of the susceptibility below T_N. Specific heat of $NdCrGeO_5$ (see the inset of Fig. 9) shows a sharp peak at ~2.5 K consistent with the susceptibility data.

The spin systems of $RCrGeO_5$ compounds include two types of magnetic atoms: $3d^3$ ($S = 3/2$) Cr^{+3} cations and rare-earth ($4f$) cations. One may think (at least, in a first approximation) that the interaction between the d and f subsystems is weak. Then, magnetic susceptibility is a sum of the contributions of the two subsystems: $\chi = \chi_d + \chi_f$. In general, f electrons of neighboring atoms are weakly coupled (for example, in the RMn_2O_5 compounds, magnetic moments of R cations order below 10 K [1–4,7]). Therefore, χ_f may be considered as the susceptibility of isolated rare-earth cations. Yet the interactions between the Cr^{+3} cations cannot be neglected.

At first glance, one would readily expect strong coupling between the Cr^{+3} cations within the structural chains (due to Cr–O–Cr and Cr–Cr exchange pathways). The interchain couplings

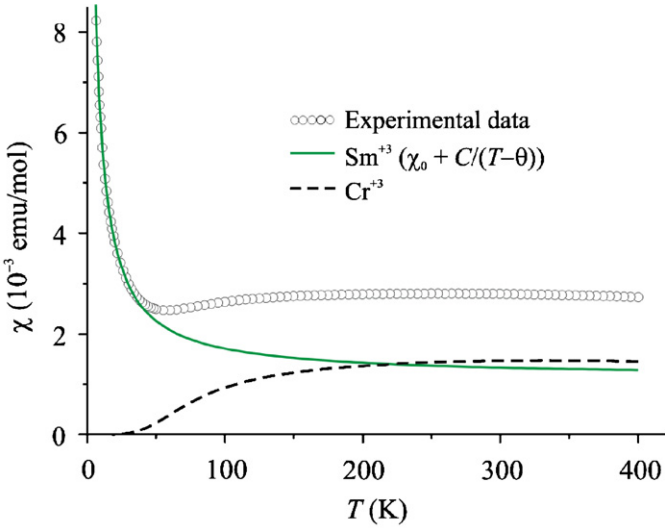

Fig. 7. Magnetic susceptibility of $SmCrGeO_5$ measured in the field $\mu_0 H = 1$ T (empty circles). The contributions of Sm^{+3} and Cr^{+3} are shown by solid and dashed lines, respectively.

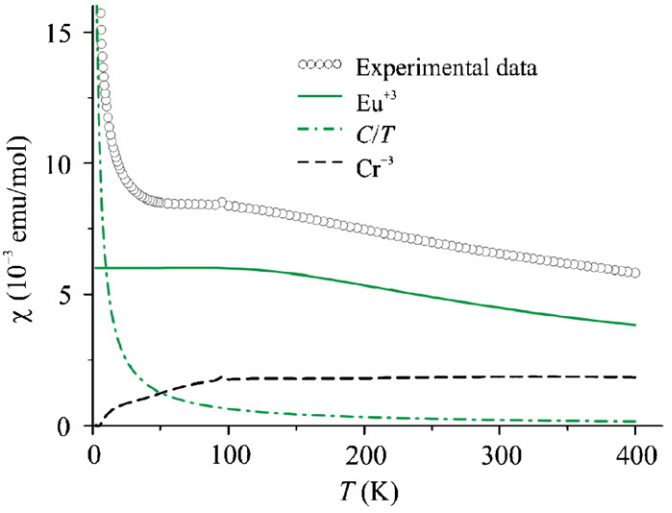

Fig. 8. Magnetic susceptibility of $EuCrGeO_5$ measured in the field $\mu_0 H = 1$ T (empty circles). The contributions of Eu^{+3}, Cr^{+3}, and paramagnetic impurities are shown by solid, dashed, and dash-dotted lines, respectively.

look weak, since the chains are separated by non-magnetic GeO_5 square pyramids. However, non-magnetic groups may effectively mediate superexchange interactions, and the situation is not that simple (an instructive example is given by $CrXO_4$ compounds with X = P, As, V^{+5}, where magnetic structure is controlled by interchain interactions via non-magnetic XO_4 groups [30]). Further on, the Cr–Cr separations alternate within the chain, therefore two different intra-chain couplings are expected. The geometrical parameters of the respective Cr–(O)–Cr pathways for R = Nd, Sm, and Eu (see Table 4) nearly match, and one may anticipate similar intra-chain interactions for all the three compounds. However, it is difficult to suggest *a priori* the signs and magnitudes of these interactions, and it is even more difficult to do any predictions for the interchain interactions.

At present, we cannot suggest a valid spin model for the *d* subsystem in $RCrGeO_5$. Therefore, the fitting of the experimental data with model expressions is not possible, and we have to turn to a simplified analysis. Below, we assume that at low temperatures $\chi_d \ll \chi_f$ (the justification is given in the end of this subsection), hence $\chi \approx \chi_f$. Thus, we fit the low-temperature data as χ_f only and use the fit to subtract the *f* contribution at higher temperatures.

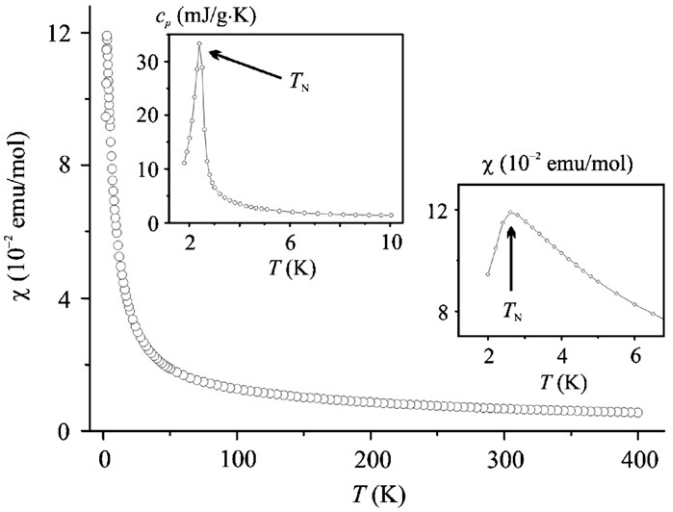

Fig. 9. Magnetic susceptibility of $NdCrGeO_5$ measured in the field $\mu_0 H = 1$ T. Upper inset shows specific heat of $NdCrGeO_5$, while the bottom one enlarges magnetic susceptibility for the low-temperature region.

The ground state of Sm^{+3} is $^6H_{5/2}$. The first excited state ($^6H_{7/2}$) lies ~1000–1500 cm^{-1} above the ground state; therefore, Sm^{+3} reveals both Curie and Van Vleck paramagnetism. At low temperatures, the Van Vleck contribution is almost temperature independent, and we fit the susceptibility of $SmCrGeO_5$ below 30 K as $\chi = \chi_0 + C/(T-\theta)$ [31]. The fit results in $\chi_0 = 1.14(4) \times 10^{-3}$ emu/mol, $C = 0.058(1)$ emu K/mol, and $\theta = -1.6(1)$ K. The value of χ_0 is slightly higher than one would expect for Sm^{+3} ($5–7 \times 10^{-4}$ emu/mol [31]), and the difference may be caused by the temperature-independent contribution of Cr^{+3} cations. The Curie constant C corresponds to $\mu_{eff} = 0.680(4)\,\mu_B$ in reasonable agreement with the expected value of $0.845\,\mu_B$ ($g_J = 2/7$) [31]. Both the χ_d and χ_f components of the susceptibility of $SmCrGeO_5$ are shown in Fig. 7.

The ground state of Eu^{+3} is $^7F_0$. The total moment is zero, therefore Eu^{+3} reveals Van Vleck paramagnetism only: χ_f increases with decreasing temperature and saturates below 100 K [31]. To estimate χ_f quantitatively, we use the expression from Ref. [31] with spin–orbit coupling constant $\lambda = 350\,cm^{-1}$. Similar to $SmCrGeO_5$, we fit the susceptibility of $EuCrGeO_5$ below 30 K as $\chi = \chi_0 + C/T$, where χ_0 is the low-temperature limit of χ_f, and C/T accounts for the upturn at low temperatures that is likely caused by impurities and defects. The fit results in $C \sim 0.045$ emu K/mol. Subtracting both χ_f and C/T from the experimental data, we find the contribution of Cr^{+3} that shows the same magnitude as in the case of $SmCrGeO_5$. Three contributions to the susceptibility of $EuCrGeO_5$ are visualized in Fig. 8.

Finally, we analyze the susceptibility of $NdCrGeO_5$. The ground state $^4I_{9/2}$ of Nd^{+3} gives rise to Curie paramagnetism with $\mu_{eff} = 3.62\,\mu_B$ ($g_J = 8/11$) [31]. However, fitting of low-temperature data (between 10 and 30 K) with Curie–Weiss law $C/(T-\theta)$ results in $C = 0.945(3)$ emu K/mol, $\theta = -5.9(2)$ K, i.e., the effective moment of Nd^{+3} is $2.75\,\mu_B$ in rather bad agreement with the expected value of $3.62\,\mu_B$. Moreover, the contribution of Cr^{+3} above 100 K was found to be $\sim 4 \times 10^{-3}$ emu/mol exceeding that in $SmCrGeO_5$ and $EuCrGeO_5$ at least by a factor of 2 (Fig. 10). One may think that the interactions between Nd^{+3} cations lead to the deviation from the Curie–Weiss law at low temperatures and result in the incorrect fitting. To test this hypothesis, we

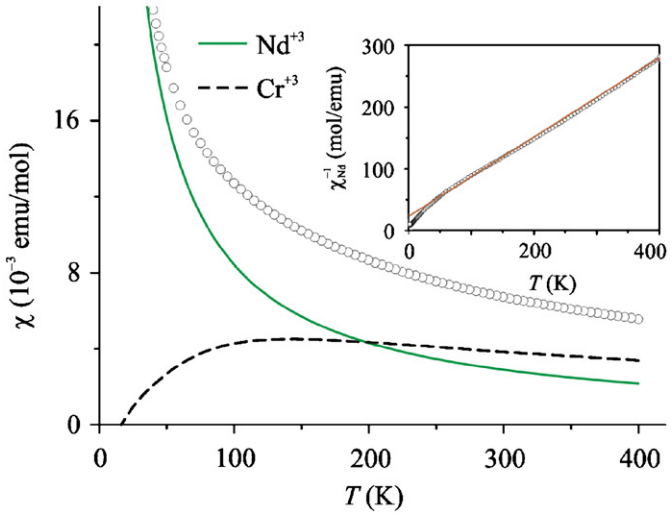

Fig. 10. Magnetic susceptibility of $NdCrGeO_5$ measured in the field $\mu_0 H = 1$ T (empty circles). The contributions of Nd^{+3} and Cr^{+3} are shown by solid and dashed lines, respectively. The inset presents $1/\chi_{Nd}$ calculated by the subtraction of χ_d for $SmCrGeO_5$ from the experimental susceptibility for $NdCrGeO_5$, solid line indicates the respective Curie–Weiss fit (see text for details).

subtracted χ_d of $SmCrGeO_5$ and $EuCrGeO_5$ from the experimental susceptibility of $NdCrGeO_5$. The resulting χ_f perfectly fits Curie–Weiss law above 50 K (see the inset of Fig. 10), and $\mu_{eff} = 3.5$–$3.6\,\mu_B$ is in remarkable agreement with the expected effective moment of Nd^{+3}. Note however that $\theta \sim -30$ K may be too high as compared with the Néel temperature of 2.5 K. Nevertheless, the above results clearly indicate that χ_d in $NdCrGeO_5$ is similar to that in $SmCrGeO_5$ or $EuCrGeO_5$, and the first fit with the underestimated effective moment of Nd^{+3} is incorrect.

Thus, we succeeded to analyze the susceptibility data for the three $RCrGeO_5$ compounds in a rough, semi-quantitative manner. The initial assumption ($\chi_d \ll \chi_f$ at low temperatures) is justified by the reasonable values for the effective moments of Sm^{+3} and Nd^{+3}. In case of $EuCrGeO_5$, we chose an appropriate λ [31] and found χ_d similar to that of $SmCrGeO_5$. Now, we compare the resulting χ_d with the susceptibility of non-interacting Cr^{+3} cations. The spin-only effective magnetic moment of a spin-3/2 cation is $3.87\,\mu_B$, and the susceptibility of the non-interacting cations (χ_{para}) will be as large as 4.7×10^{-3} emu/mol even at 400 K, i.e., exceeding χ_d by a factor of 3. Thus, χ_d is strongly reduced as compared with χ_{para}. One may arrive to the same conclusion by a simple consideration of the susceptibility data for $SmCrGeO_5$. The magnetic moment of Sm^{+3} is rather small, and the Cr^{+3} contribution should be well pronounced. Above 50 K, the total susceptibility equals $\sim 3 \times 10^{-3}$ emu/mol, well below the values expected for the non-interacting Cr^{+3} cations in this temperature range.

The latter result implies that the Cr^{+3} cations in the $RCrGeO_5$ compounds are coupled antiferromagnetically. Moreover, these cations should be ordered in the crystal structure, since structural disorder (particularly, mixing of magnetic and non-magnetic cations within one position) usually suppresses magnetic interactions and leads to strong Curie-like contribution to the magnetic susceptibility (see, for example, [32]).

4. Discussion

$RCrGeO_5$ germanates present new examples of RMn_2O_5-type compounds. Chromium atoms occupy octahedral positions (like Mn^{4+} or Al^{3+}), while germanium ones are placed in the square pyramid (like Mn^{3+}). Note that the RMn_2O_5 compounds were synthesized for all rare-earth cations as well as for yttrium and bismuth [10,20], whereas $RCrGeO_5$ germanates could be prepared for a limited number of R only (Nd–Er). The different stability of RMn_2O_5 and $RCrGeO_5$ oxides may be explained by different nature of the B-type cations and their different ability to adopt to a change of A-cation size. The size of the octahedrally coordinated cation becomes larger in $RCrGeO_5$ as compared with that in RMn_2O_5 (0.755 vs. 0.68 Å), while the size of the penta-coordinated cation is strongly reduced (0.60 vs. 0.72 Å). These changes should lead to noticeable stresses in the structure and, consequently, to the rigid restrictions for the R-cation size.

The key fragment of the RMn_2O_5 structure is shown in Fig. 4. One may see that there are two different cation separations (D_1 and D_2) in the chains of edge-sharing octahedra. D_2 is constrained

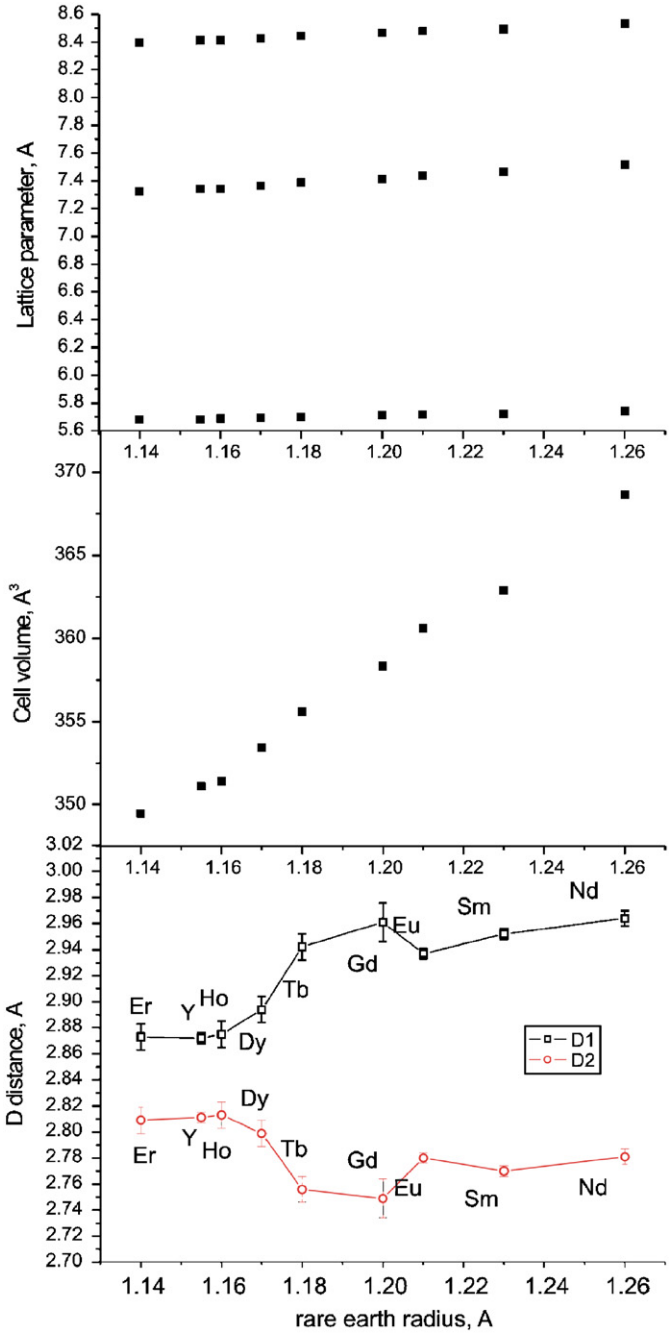

Fig. 11. Lattice parameters, cell volume, and Cr–Cr separations vs. ionic radius of the rare-earth cation for the $RCrGeO_5$ compounds.

by the edge of the square pyramid (O(4)–O(4)) that shares corners with the respective octahedra, while D_1 is more flexible. Basically, D_2 lies in the range of 2.75–2.80 Å for most of the RMn$_2$O$_5$-type compounds. The separation of ~2.80 Å is normal for small aluminum cations, therefore $D_1 \sim D_2 \sim 2.80$ Å in RAlGeO$_5$ [15,16]. Larger Mn^{+4} and Cr^{+3} cations require larger separations, hence D_1 is expanded, and the expansion is controlled by the R cation size.

The values of D_1 and D_2 for RCrGeO$_5$ are listed in Table 4, and their dependence on the radius of the rare-earth cation (r_R) is shown in the bottom panel of Fig. 11. In general, the difference between D_1 and D_2 is decreased with the decrease of r_R. However, the monotonic behavior is slightly broken by gadolinium and terbium. Similar dependence for the Mn−Mn separations was observed in the structures of the RMn$_2$O$_5$ compounds as well [12,33]. Yet the reason of the Gd and Tb anomaly is not clear. The lattice parameters and cell volume for RCrGeO$_5$ almost linearly depend on r_R (Fig. 11). The linear change of the c parameter should lead to linear behavior of (D_1+D_2) vs. r_R, while the individual distances D_1 and D_2 are more flexible and show non-linear behavior.

One may suggest a reason why the RCrGeO$_5$ compounds are formed for R = Nd–Er only, whereas the RMn$_2$O$_5$ oxides have been reported for all the rare-earth elements. The main factor which influences on the D_1 value is the size of the rare-earth element, while the D_2 separation is almost fixed by the rigid GeO$_5$ pyramids. The Nd^{+3}, Sm^{+3}, and Eu^{+3} cations provide $D_2 \sim 2.80$ Å, $D_1 \sim 2.95$ Å that seems to be optimal for the Cr−Cr chains in RCrGeO$_5$. Larger rare-earth cations (La, Ce, Pr) should also be favorable for Cr^{+3}, but they may be too large for the framework restricted by the small GeO$_5$ pyramids. In case of small R cations (Tm–Lu), the D_1 separation likely becomes too short for the relatively large Cr^{+3}.

A great variety of cations can be introduced into the RMn$_2$O$_5$-type structure, but the problem of the cation disorder arises. The size difference should prevent the cations from antisite disorder; therefore, the Cr^{+3}/Ge^{+4} ordering observed in RCrGeO$_5$ is quite natural. However, a mismatch of the cation sizes causes stresses in the RMn$_2$O$_5$-type structure and limits the set of the appropriate R cations. Thus, the choice of the cations for the preparation of novel magnetoelectric RMn$_2$O$_5$-type compounds is a very subtle issue. One should probably think about the accommodation of a large atom in the square pyramid and $D_1 \sim D_2$ (or even $D_1 < D_2$) regime. In this case, D_2 should not cause any notable stress for the octahedrally coordinated atom, while D_1 will provide flexibility towards the change of the R cation size. In particular, we think that V^{+4} could be an optimal choice for the cation in the square pyramid. Note that V^{+4} favors square-pyramidal (or distorted octahedral) coordination [34], and this effect may additionally prevent the structure from the antisite disorder.

In the following, we will focus on the magnetic properties of the RCrGeO$_5$ germanates. Clearly, the introduction of non-magnetic Ge^{+4} breaks frustrated spin system of RMn$_2$O$_5$ and destroys intriguing magnetoelectric properties of these compounds. In this sense, our results are similar to the recent report on the preparation and magnetic properties of YGa$_{1-x}$Mn$_{1+x}$O$_5$ [17]. According to [17], the introduction of non-magnetic cations could simplify magnetic interactions between Mn cations, hence, facilitating our understanding of exchange couplings in the RMn$_2$O$_5$ structure type. We are convinced that studying of the RCrGeO$_5$ compounds may also be helpful for this purpose. Yet we should emphasize an essential difference concerning the manifestation of magnetic interactions in RCrGeO$_5$ and YGa$_{1-x}$Mn$_{1+x}$O$_5$.

Our analysis of the magnetic susceptibility data indicates the presence of antiferromagnetic couplings between the Cr^{+3} cations. The reduction of the susceptibility (as compared with that for the non-interacting case) is well pronounced even at 400 K, hence the interactions are quite strong. The typical energy scale of super-exchange couplings running via non-magnetic groups (such as GeO$_5$ pyramids) is below 100–150 K [35], while the Cr–(O)–Cr pathways may provide stronger couplings. Therefore, we can safely claim that the strongest interactions run within the structural chains, and the spin system is basically one dimensional. Two alternating intra-chain interactions are present in RCrGeO$_5$, and at least one of these interactions should be antiferromagnetic. This result contrasts with the recent study of an isostructural compound YGa$_{1-x}$Mn$_{1+x}$O$_5$ that shows ferromagnetic ordering below 100 K [17].

To understand the difference between RCrGeO$_5$ and YGa$_{1-x}$Mn$_{1+x}$O$_5$, one should consider the intra-chain magnetic interactions. The relevant pathways are M–(O)–M ($M = Cr^{+3}$ or Mn^{+4}) ones with the M–O–M angle close to 90° (see Table 4). According to Goodenough–Kanamori rules, the sign of the coupling is determined by a competition of antiferromagnetic (due to the direct M–M exchange) and ferromagnetic (due to 90° M–O–M superexchange) contributions. Both the magnetic cations have similar electronic configuration $3d^3$. The cation separations D_2 are also similar, while YGa$_{1-x}$Mn$_{1+x}$O$_5$ reveals a smaller D_1 as compared with that of the RCrGeO$_5$ compounds with R = Nd, Sm, and Eu (2.88 vs. ~2.94 Å). The change of D_1 is reasonable, since Cr^{+3} is larger than Mn^{+4}. Yet D_2 remains nearly constant due to the constraint imposed by the square pyramids. Therefore, the direct overlap of the cation d orbitals (i.e., the M–M exchange) in the chromium compounds is enhanced, and the antiferromagnetic contribution is also enhanced resulting in the overall antiferromagnetic behavior of RCrGeO$_5$. Note however that our data do not provide any information about the second intra-chain coupling (one corresponding to D_1) that may be either ferro- or antiferromagnetic.

The strong magnetic interactions in the RCrGeO$_5$ compounds contrast with the lack of long-range ordering for R = Sm, Eu and the very low transition temperature for R = Nd. One may think that either the interchain interactions are very weak or these interactions are frustrated. The latter case is reminiscent of CrXO$_4$ (X = P, As, V^{+5}) compounds [30]. We believe that the magnetic properties of RCrGeO$_5$ are somewhat unusual and look forward to the further studies of the subject.

In conclusion, we have prepared a number of novel complex germanates RCrGeO$_5$ (R = Nd–Er, Y) and investigated these compounds with XPD, electron microscopy, and physical properties measurements. RCrGeO$_5$ germanates present new examples of RMn$_2$O$_5$-type compounds and show cation ordering (Cr^{+3} in the octahedron and Ge^{+4} in the square pyramid) due to the different size of Cr^{+3} and Ge^{+4}. The mismatch of the cation sizes decreases the stability of the RMn$_2$O$_5$ structure; therefore, RCrGeO$_5$ can be prepared for a limited number or rare-earth cations only. Magnetic susceptibility measurements for three of the prepared compounds (R = Nd, Sm, and Eu) indicate strong antiferromagnetic coupling between the Cr^{+3} cations. NdCrGeO$_5$ undergoes long-range magnetic ordering at 2.6 K.

Acknowledgment

The authors are grateful to RFBR (Grant 07-03-00890) for financial support. R.Sh. is grateful to NIMS for granting his stay. A.Ts. acknowledges the hospitality of MPI CPfS (Dresden) and the financial support. Part of this work has been performed within the framework of the IAP V-1 of the Belgian government.

Appendix A. Supplementary materials

The online version of this article contains additional supplementary data. Please visit doi:10.1016/j.jssc.2008.05.043.

References

[1] N. Hur, S. Park, P.A. Sharma, J.S. Ahn, S. Guha, S.-W. Cheong, Nature 429 (2004) 392.
[2] N. Hur, S. Park, P.A. Sharma, S. Guha, S.-W. Cheong, Phys. Rev. Lett. 93 (2004) 107207.
[3] L.C. Chapon, G.R. Blake, M.J. Gutmann, S. Park, N. Hur, P.G. Radaelli, S.-W. Cheong, Phys. Rev. Lett. 93 (2004) 177402.
[4] D. Higashiyama, S. Miyasaka, N. Kida, T. Arima, Y. Tokura, Phys. Rev. B 70 (2004) 174405.
[5] L.C. Chapon, P.G. Radaelli, G.R. Blake, S. Park, S.-W. Cheong, Phys. Rev. Lett. 96 (2006) 097601.
[6] D. Higashiyama, S. Miyasaka, Y. Tokura, Phys. Rev. B 72 (2005) 064421.
[7] W. Ratcliff II, V. Kiryukhin, M. Kenzelmann, S.-H. Lee, R. Erwin, J. Schefer, N. Hur, S. Park, S.-W. Cheong, Phys. Rev. B 72 (2005) 060407.
[8] J. Okamoto, D.J. Huang, C.-Y. Mou, K.S. Chao, H.-J. Lin, S. Park, S.-W. Cheong, C.T. Chen, Phys. Rev. Lett. 98 (2007) 157202.
[9] A.B. Sushkov, R.V. Aguilar, S. Park, S.-W. Cheong, H.D. Drew, Phys. Rev. Lett. 98 (2007) 027202.
[10] A. Muñoz, J.A. Alonso, M.T. Casais, M.J. Martínez-Lope, J.L. Martínez, M.T. Fernández-Diaz, Phys. Rev. B 65 (2002) 144423.
[11] A. Muñoz, J.A. Alonso, M.T. Casais, M.J. Martínez-Lope, J.L. Martínez, M.T. Fernández-Diaz, Eur. J. Inorg. Chem. (2005) 685.
[12] M. Tachibana, K. Akiyama, H. Kawaji, T. Atake, Phys. Rev. B 72 (2005) 224425.
[13] (a) A. Muñoz, J.A. Alonso, M.J. Martínez-Lope, J.L. Martínez, Chem. Mater. 16 (2004) 4087;
(b) A. Muñoz, J.A. Alonso, M.J. Martínez-Lope, J.L. Martínez, Phys. Rev. B 72 (2005) 184402;
(c) A. Muñoz, J.A. Alonso, M.J. Martínez-Lope, J.L. Martínez, Eur. J. Inorg. Chem. (2007) 1972.
[14] J.A. Alonso, M.J. Martínez-Lope, M.T. Casais, J.L. Martínez, V. Pomjakushin, Eur. J. Inorg. Chem. (2005) 2600.
[15] (a) O. Jarchow, K.H. Klaska, M. Werk, Naturwissenschaften 68 (1981) 92;
(b) O. Jarchow, K.H. Klaska, M. Werk, Z. Kristallogr. 154 (1981) 341;
(c) O. Jarchow, K.H. Klaska, M. Werk, Z. Kristallogr. 159 (1982) 65.
[16] A. Durand, O. Mentre, F. Abraham, T. Fukuda, B. Elouadi, Solid State Sci. 8 (2006) 155.
[17] C. de la Calle, J.A. Alonso, M.J. Martínez-Lope, M. García-Hernández, G. André, Mater. Res. Bull. 43 (2008) 197.
[18] (a) A.C. Larson, R.B. Von Dreele, Los Alamos National Laboratory Report LAUR 86-748 (1994);
(b) B.H. Toby, J. Appl. Crystallogr. 34 (2001) 210.
[19] R.D. Shannon, Acta Crystallogr. A 32 (1976) 751.
[20] (a) G. Popov, M. Greenblatt, W.H. McCarroll, Mater. Res. Bull. 35 (2000) 1661;
(b) J.A. Alonso, M.T. Casais, M.J. Martínez-Lope, I. Rasines, J. Solid State Chem. 129 (1997) 105;
(c) J.A. Alonso, M.T. Casais, M.J. Martínez-Lope, J.L. Martínez, M.T. Fernández-Díaz, J. Phys.: Condens. Matter 9 (1997) 8515.
[21] P. Euzen, P. Leone, C. Gueho, P. Palvadeau, Acta Crystallogr. C 49 (1993) 1875.
[22] W.-J. Zhu, P.H. Hor, J. Solid State Chem. 134 (1997) 128.
[23] M. Ardon, S. Cohen, Inorg. Chem. 32 (1993) 3241.
[24] I.D. Brown, D. Altermatt, Acta Crystallogr. B 41 (1985) 244.
[25] G. Adiwidjaja, M. Broeker, C. Claus, K. Friese, K.H. Klaska, O. Jarchow, M. Ruks, I. Wozniak, Z. Kristallogr. 213 (1998) 223.
[26] M. Behruzi, K.H. Breuer, W. Eysel, Z. Kristallogr. 176 (1986) 205.
[27] B. Harbrecht, J. Kushauer, H.-J. Weber, Eur. J. Solid State Inorg. Chem. 27 (1990) 831.
[28] E. Cuno, Hk. Müller-Buschbaum, Z. Anorg. Allg. Chem. 564 (1988) 26.
[29] R.M. Hornreich, J. Magn. Magn. Mater. 7 (1978) 280 and references therein.
[30] (a) J.P. Attfield, P.D. Battle, A.K. Cheetham, J. Solid State Chem. 57 (1985) 357;
(b) J.P. Attfield, A.K. Cheetham, D.C. Johnson, C.C. Torardi, Inorg. Chem. 26 (1987) 3379;
(c) J.P. Wright, J.P. Attfield, W.I.F. David, J.B. Forsyth, Phys. Rev. B 62 (2000) 992 and references therein.
[31] (a) G.F. Goya, R.C. Mercader, M.T. Causa, M. Tovar, J. Phys.: Condens. Matter 8 (1996) 8607;
(b) K. Tezuka, Y. Hinatsu, N.M. Masaki, M. Saeki, J. Solid State Chem. 138 (1998) 342;
(c) M. Wakeshima, D. Harada, Y. Hinatsu, N. Masaki, J. Solid State Chem. 147 (1999) 618;
(d) Y. Doi, Y. Hinatsu, J. Phys.: Condens. Matter 13 (2001) 4191.
[32] K.M. Kojima, J. Yamanobe, H. Eisaki, S. Uchida, Y. Fudamoto, I.M. Gat, M.I. Larkin, A. Savici, Y.J. Uemura, P.P. Kyriakou, M.T. Rovers, G.M. Luke, Phys. Rev. B 70 (2004) 094402.
[33] I. Kagomiya, K. Kohn, T. Uchiyama, Ferroelectrics 280 (2002) 131.
[34] P.Y. Zavalij, M.S. Whittingham, Acta Crystallogr. B 55 (1999) 627.
[35] (a) R. Valenti, T. Saha-Dasgupta, C. Gros, Phys. Rev. B 66 (2002) 054426;
(b) A. Zheludev, G. Shirane, Y. Sasago, N. Kiode, K. Uchinokura, Phys. Rev. B 54 (1996) 15163.